Magnesium Technology 2011
Edited by: Wim H. Sillekens, Sean R. Agnew, Neale R. Neelameggham, and Suveen N. Mathaudhu
TMS (The Minerals, Metals & Materials Society), 2011

EFFECTS OF SILICON CARBIDE NANOPARTICLES ON MECHANICAL PROPERTIES AND MICROSTRUCTURE OF AS-CAST Mg-12wt.%Al-0.2wt.%Mn NANOCOMPOSITES

Hongseok Choi; Hiromi Konishi; Xiaochun Li
Mechanical Engineering Department, University of Wisconsin-Madison, Madison, WI 53706, USA

Keywords: Mg-Al alloy, Nanocomposite, Grain refining, Intermetallic phase, Ductility

Abstract

Microstructure and tensile properties of as-cast Mg-12Al-0.2Mn alloys with SiC nanoparticles were studied. SiC nanoparticles were dispersed into Mg-12Al-0.2Mn melts through an ultrasonic based nanoparticle-dispersion method. The content of SiC nanoparticles varied from 0 to 2 wt.%. The microstructural analysis with optical and scanning electron microscopy (SEM) showed that the massive brittle intermetallic phase (β-$Mg_{17}Al_{12}$) as well as α-Mg grain was significantly refined, enhancing both strengths and ductility of as-cast Mg-12Al-0.2Mn alloys. Transmission electron microscopy (TEM) showed that there were SiC nanoparticles in both α-Mg and β-$Mg_{17}Al_{12}$ phases of the Mg-12Al-0.2Mn nanocomposites. It was found that there was a partial reaction between Mg/Al and SiC nanoparticles, producing Mg_2Si intermetallic phases. X-ray diffraction (XRD) analysis confirmed also that the content of Mg_2Si phases increased with increasing SiC content, limiting a further ductility enhancement for Mg-12Al-0.2Mn-SiC nanocomposite.

Introduction

Magnesium alloys are of great potential as structural materials. The demand for magnesium is continuously increasing due to the effort by automotive industry to use lighter metals to reduce fuel consumption and achieve lower emission levels. Moreover, magnesium alloys are also utilized widely in electric and aerospace industries, etc. The most applicable alloys are those based on Mg-Al, such as AZ91, because of their excellent castability, corrosion resistance, and strength at room temperature [1-4]. Furthermore, AZ91 is the Mg-Al alloys with the highest Al content for commercial applications today. It is well-known that the strength of the Mg-Al alloys is improved as the Al content increases. However, the ductility decreases significantly with increased Al content, which limits applications of the alloys.

The high strength of alloys can also be attained from grain refinement because grain size is one of the most important factors determining the mechanical properties of Mg alloys according to Hall-Petch equation [5]. There are a variety of different methods to achieve refined grains in alloys: by increasing the cooling rate, adding heterogeneous nuclei during solidification processing, etc [6]. Although much research has been reported in achieving fine grains in various Mg alloys [7-10], reliable and castable Mg-Al alloys with higher Al content still remain to be further grain refined and developed so that their potential higher mechanical strength can be utilized for commercial applications.

Recently, there have been increasing studies about a new class of nanostructured materials, Mg metal matrix nanocomposites (Mg MMNCs), consisting of Mg alloys reinforced with ceramic nanoparticles, due to their potential to strengthen the Mg matrix while maintaining or even enhancing ductility [11-14]. Ceramic materials, e.g. silicon carbide (SiC) and aluminum oxide (Al_2O_3), have been widely used as reinforcement particles in aluminum alloys due to their relatively good thermal and chemical stability as compared to other types of reinforcements [15, 16]. However, most processing techniques are not capable of producing bulk nanocomposites of complex shapes. Solidification processing, e.g. casting, is a desirable processing method. However, it is extremely difficult to uniformly disperse nanoparticles in metal melts due to their high specific surface areas, which easily induce agglomeration and clustering. A novel technique, ultrasonic-cavitation based solidification processing, was recently developed, and it was found that nanoparticles had a significant effect on the properties and microstructure of alloys [12-14].

The purpose of this study is to investigate the effect of ceramic nanoparticles on microstructure of Mg alloys with higher Al content in order to produce as-cast high performance Mg-Al alloys with much improved ductility. The mechanical properties of Mg-Al nanocomposites will also be tested and the mechanisms of properties change will be discussed based on the microstructure analysis.

Experimental Procedure

Commercial pure magnesium (99.9% purity), pure aluminum (99.8% purity), and aluminum-manganese master alloy (25wt.% Mn) were used to synthesize Mg-Al alloys. The Mg alloy with higher Al content (Mg-12wt.%Al-0.2wt.%Mn alloys in this study) were chosen as the matrix materials. β-SiC nanoparticles (97.5% purity; Si<0.15, Cl<0.15, C<0.75, O<1.25wt.%) with an average size of 50 nm (Nanostructured & Amorphous Materials, Inc., USA) were used for the nanocomposites of Mg-12Al-0.2Mn alloy through an innovative ultrasonic-cavitation based dispersion method developed earlier [12].

The processing procedure for casting nanocomposites includes melting the alloy, creating ultrasonic cavitation and streaming in the molten metal by an ultrasonic processing system, addition of preheated nanoparticles (150 °C for one hour), and casting the nanocomposite melt into a permanent mold. Figure 1 shows the schematics of experimental set-up for the ultrasonic-cavitation based dispersion processing of SiC nanoparticles for Mg-12Al-0.2Mn nanocomposites. The system consists of a resistance heating furnace to melt the alloys, a nanoparticle feeding system, gas protection system and an ultrasonic processing system. The ultrasonic processing system consists of an ultrasonic probe, booster and transducer. A niobium ultrasonic probe with a diameter of 12.7 mm and a length of 92 mm was attached to a booster (Sonicator 3000, Misonix, USA), which was mounted in a transducer working under a frequency of 20 kHz and a maximum power output of 600 W.

About 160 g of magnesium alloy was melted in a mild steel crucible under a protective CO_2+1%SF_6 gas. The tip of a niobium ultrasonic probe was inserted into the melt about 12.7 mm in

depth when the melt temperature dropped to an ultrasonic processing temperature at about 700 °C. Ultrasonic vibrations with a peak-to-peak amplitude of 60 μm were used, and then nanoparticles were added into the melt during ultrasonic processing.

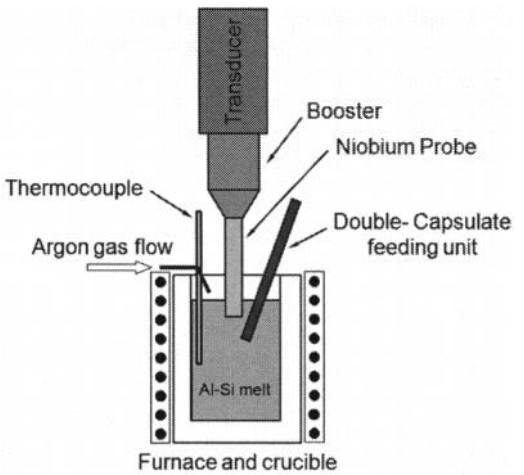

Figure 1. Schemetic of experimental set-up for ultrasonic processing.

Due to a low specific density of ceramic nanoparticles and their poor wettability with metal melt, the ceramic nanoparticles tend to float to the melt surface at first before ultrasonic cavitation helps to mix them into the melts. Therefore, an effective feeding technique (double-capsulate feeding method) was developed to improve feeding efficiency. In the double-capsulate feeding method, ceramic nanoparticles were first wrapped with a thin aluminum foil (Alloy 1000) with a thickness of 0.0127 mm, and then the aluminum foil was rolled up into a rod shape with a diameter of about 6 mm (making the first capsule). The aluminum foil rod was wrapped again with another thin aluminum foil (Alloy 1100) with a dimension of 355.6 mm × 152.4 mm and a thickness of 0.0254 mm (making the second capsule). The second aluminum foil would make the nanoparticles discharge into the melt gradually, resulting from the graduate melting of the thicker wall of the capsule. The aluminum foil capsule with a total weight of 4.6 g containing ceramic nanoparticles was then put into the melt during ultrasonic processing. One Al foil capsule was slowly fed into the melt and ultrasonically processed within the melt. The melt was ultrasonically processed for 10 minutes for each Al foil capsule, bringing a total processing time of 30 minutes. After the ultrasonic processing for 30 minutes, the ultrasonic probe was lifted out of the melt and the temperature of the melt was increased to 740 °C for pouring. The melt was cast into a low carbon steel permanent mold preheated to 400 °C. Two standard flat tensile specimens with a gage dimension of 6.35 mm × 6.35 mm and a gage length of 38.1 mm were obtained after each casting. For comparison reasons, samples were also made without nanoparticle additions (but still with aluminum foils and capsule of the same amount as in the nanocomposites).

Mechanical properties of samples were determined using a tensile testing machine (SINTECH 10/GL, MTS, USA) with a crosshead speed of 5.08 mm/minute. For accurate measurement of yield strength, an extensometer was used for up to 0.2% strain at which point the test was paused, and the extensometer was removed. Final elongation was measured manually after putting the two test bar pieces back together according to ASTM B 557-06. The microstructural characterization was conducted with polished samples of pure alloy and its nanocomposites. They were lightly etched using a 2% natal etchant. Optic microscope and Scanning Electron Microscopy (SEM) with Energy Dispersive X-ray spectroscopy (EDS) were used for detailed metallographic analysis. Transmission Electron Microscopy (TEM) samples were prepared using ion milling. The TEM analysis of samples was conducted using a FEI TITAN-80-200 microscope, operating at an accelerating voltage of 200 kV. X-ray diffraction (XRD) measurements were done using a Scintag Pad V Diffractometer with CuKα radiation. The alloy samples were polished with a 1 μm diamond paste. Scan parameters used were 2θ angle 10-80 degrees, step size 0.02 degrees and dwell time of 12 seconds.

Experimental Results and Discussion

The mechanical properties of as-cast pure Mg-12Al-0.2Mn alloy and nanocomposites with two different contents of β-SiC (0.9 wt.% and 1.4 wt.%) are shown in Figure 2. The results show increases in strength (ultimate tensile and yield) and ductility of the Mg-12Al-0.2Mn alloy with the addition of β-SiC nanoparticles. For Mg-12Al-0.2Mn-0.9SiC nanocomposite, the ultimate tensile strength and yield strength are increased by 14% and 8% respectively, compared with the pure alloy. The ductility is improved from 0.97% to 1.65% (increased by 71%). This implies that β-SiC nanoparticle is effective for the enhancement of mechanical properties (especially ductility) of Mg-Al alloys with higher contents of Al. The increase in ductility with the addition of nanoparticles is in contrast to the ductility decrease that is usually seen with the addition of micro particles or fibers to metal matrix [17]. As the content of β-SiC nanoparticles increases to 1.4 wt.%, the yield strength is increased not much, only about 2% higher than that of Mg-12Al-0.2Mn-0.9SiC nanocomposite. Moreover, the ultimate tensile strength and ductility are even lower by 5% and 40% than those of Mg-12Al-0.2Mn-0.9SiC nanocomposite respectively. However, it still shows significantly increased ultimate tensile strength and ductility than the pure alloy (increased by 9% and 22% respectively).

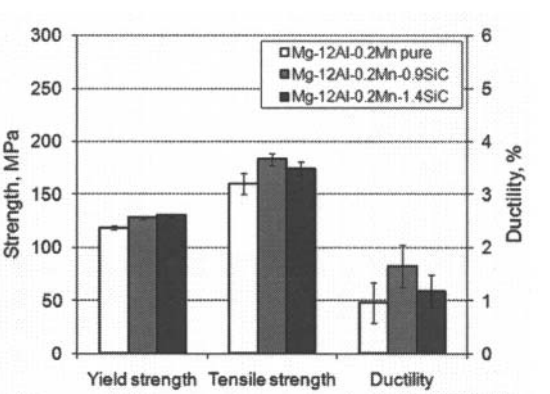

Figure 2. Mechanical properties of Mg-12Al-0.2Mn alloy and its nanocomposites.

The optical micrographs of the pure Mg-12Al-0.2Mn alloys and their nanocomposites samples are shown in Fig. 3a-c. The pure

Mg-12Al-0.2Mn alloy exhibited massive intermetallic phases (β-$Mg_{17}Al_{12}$) surrounding the primary magnesium (α-Mg) dendrites. The β-$Mg_{17}Al_{12}$ phases are mainly distributed along the boundaries of primary α-Mg grains, and have a morphology of long continuous network. Moreover, the formation of α-Mg islands of a few microns was observed inside the irregularly networked β-$Mg_{17}Al_{12}$ phases. A certain amount of lamella phases are also observed around the massive β-$Mg_{17}Al_{12}$ phases in the boundaries of primary α-Mg grains.

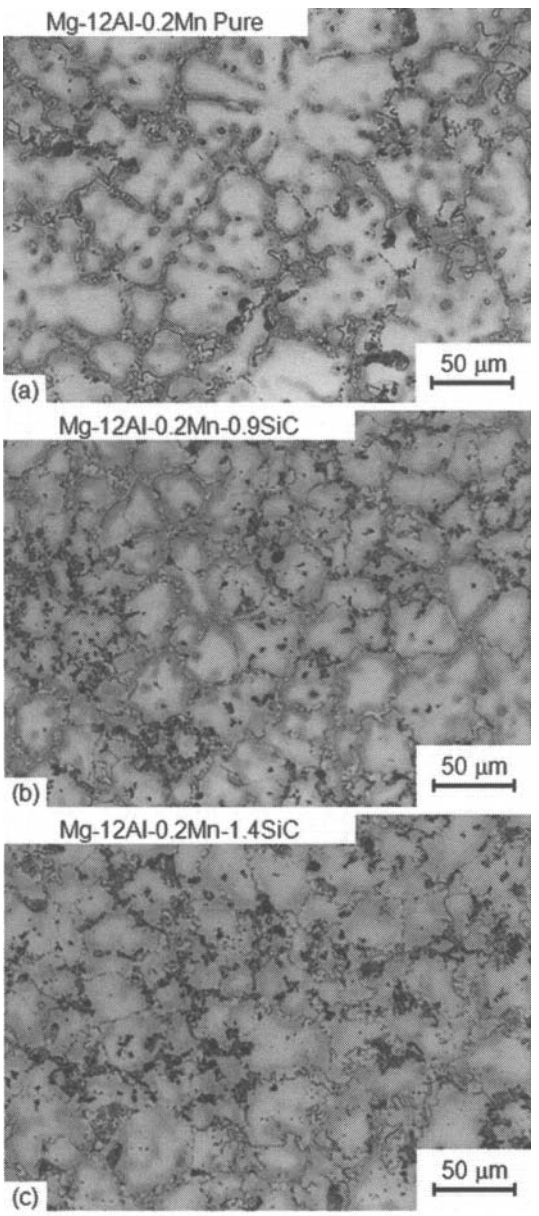

Figure 3. Optical micrographs of Mg-12Al-0.2Mn alloy modified with (a) 0% (b) 0.9% (c) 1.4% SiC nanoparticles.

Average grain size was measured using the linear intercept method from optical micrographs of the samples according to ASTM E 112-96. The grain size was 45.9 ± 7.1 μm, as shown in Fig. 4. However, figure 3b and c show that the Mg-12Al-0.2Mn nanocomposites with SiC nanoparticles have much finer globular primary α-Mg grains. With the addition of β-SiC nanoparticles, the morphology of α-Mg phases changes from large dendrite to small equiaxed globular structure. Figure 4 shows that the average size of primary α-Mg grains was noticeably reduced as compared with that of pure alloy (decreased by 52% in Mg-12Al-0.2Mn-1.4SiC nanocomposite). This is in full agreement with the previous studies [12-14], which reported that β-SiC nanoparticles would work as heterogeneous nucleation agents despite the large disregistry between Mg and β-SiC. It can be also seen from Fig. 3b and c that the β-$Mg_{17}Al_{12}$ phases in the nanocomposites are significantly modified form large continuous network to thinner and shorter structures, compared with that in the pure alloy. This might be attributed to the significant grain refinement, resulting from enhanced nucleation of α-Mg and β-$Mg_{17}Al_{12}$ phases caused by the dispersed β-SiC nanoparticles.

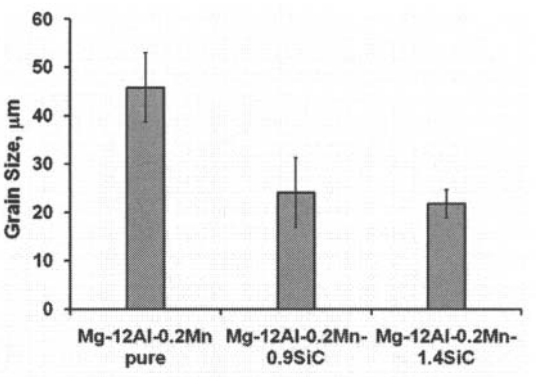

Figure 4. Average grain size of Mg-12Al-0.2Mn pure alloy and its SiC nanocomposites.

The modification of β-$Mg_{17}Al_{12}$ phases are more obviously shown in Fig. 5. Typical large continuous network of β-$Mg_{17}Al_{12}$ phases are observed in the pure Mg-12Al-0.2Mn alloy. As shown in Fig. 5a, the primary α-Mg phases of pure Mg-12Al-0.2Mn alloy have dendritic structures, and the β-$Mg_{17}Al_{12}$ phases are in the form of large continuous network with distributed small α-Mg islands. The β-$Mg_{17}Al_{12}$ phases are also formed in areas between the secondary dendrite arms, but the morphology mainly appears in a compact globular form. In the case of 0.9 wt. % SiC nanocomposites, the morphology of primary α-Mg shows typical globular equiaxed shape as shown in Fig. 5b. Some β-SiC nanoparticles micro-clusters are also observed inside the β-$Mg_{17}Al_{12}$ phases. The modification effect of β-SiC nanoparticles on the primary α-Mg is more obvious than the one on the β-$Mg_{17}Al_{12}$ phases. With higher amount of β-SiC nanoparticles (Fig. 5c), the β-$Mg_{17}Al_{12}$ phases are significantly refined. It can be found that the large long networks around primary α-Mg grains are modified to the thin and shortly discrete ones. It is noticed that the micro-clusters β-SiC nanoparticles are more easily observed in β-$Mg_{17}Al_{12}$ phases of Mg-12Al-0.2Mn-1.4SiC nanocomposite. Moreover, there is no significant change in the average grain size of α-Mg phases between two nanocomposites with different contents of β-SiC nanoparticles. These results indicate that higher content of β-SiC nanoparticles promote the modification of β-$Mg_{17}Al_{12}$ phases instead of the refinement of α-Mg phases. TEM micrographs of the α-Mg and β-$Mg_{17}Al_{12}$ phase areas of Mg-

12Al-0.2Mn-1.4SiC nanocomposite are shown in Fig. 6. Some β-SiC nanoparticles are located inside both α-Mg and β-$Mg_{17}Al_{12}$ phases, which is consistent with the observation in the optical micrographs in Fig. 5c. Therefore, the refinement of α-Mg phases might be attributed to the enhanced heterogeneous nucleation caused by the addition of β-SiC nanoparticles, and the modification of morphology of β-$Mg_{17}Al_{12}$ phases might be related to the addition of β-SiC nanoparticles, resulting in the geometrical constraint by increased grain boundary area as well as the restricted growth by neighboring β-SiC nanoparticles during the solidification process.

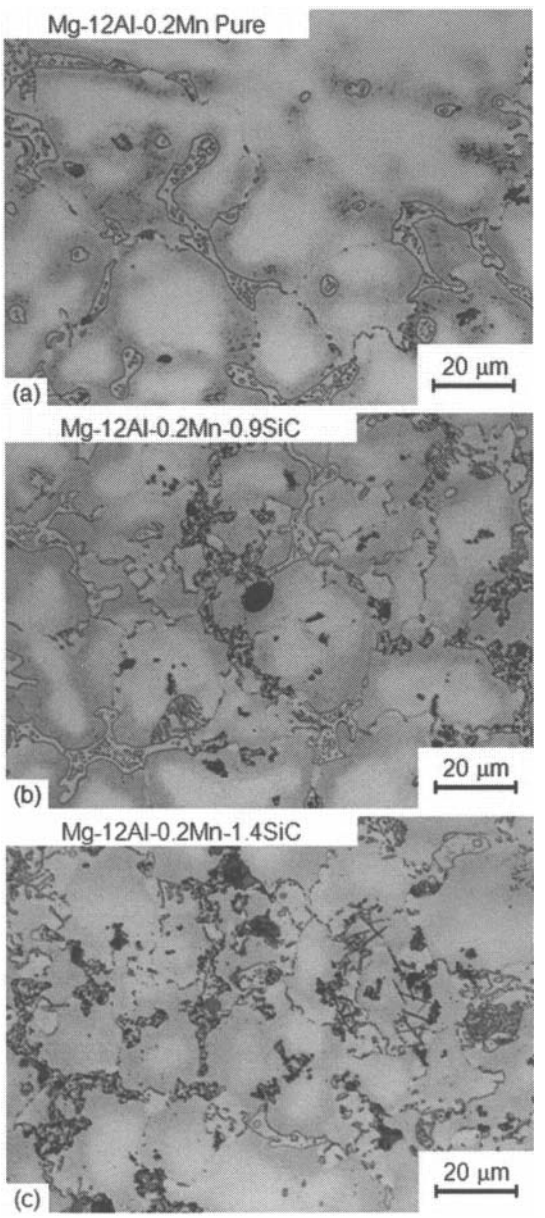

Figure 5. Optical micrographs of Mg-12Al-0.2Mn alloy modified with (a) 0% (b) 0.9% (c) 1.4% SiC nanoparticles.

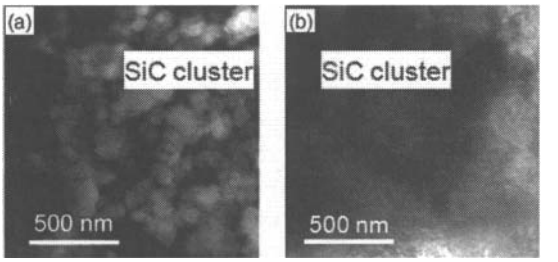

Figure 6. TEM photographs of (a) α-Mg and (b) β-SiC clusters in Mg-12Al-0.2Mn-1.4SiC nanocomposite.

The modified β-$Mg_{17}Al_{12}$ phases as well as the refined α-Mg grains would contribute to the enhancement of mechanical properties of the alloy. It is clearly shown in the experiment results that the beneficial effect of β-SiC nanoparticles on the mechanical properties of Mg-12Al-0.2Mn alloys is related to the refinement of primary α-Mg grains and modification of β-$Mg_{17}Al_{12}$ phases. The mechanical properties of cast materials typically depend on the grain size of primary and intermetallic phases. A fine microstructure means that the material contains a large amount of grain boundary area. It is well recognized in the literature that the cracks easily initiate at interfaces between the hard and brittle β-$Mg_{17}Al_{12}$ phases and α-Mg phases, and then propagate inside β-$Mg_{17}Al_{12}$ phases. The massive β-$Mg_{17}Al_{12}$ phases of body-centered cubic (b.c.c.) structure are incompatible with the primary α-Mg of hexagonal close-packed (h.c.p.) structure, which leads to the fragility of the interface of two phases. The results of the microstructural characterization show that the primary α-Mg and β-$Mg_{17}Al_{12}$ phases are refined and modified in nanocomposites. The considerable enhancement of ductility might be related to the combined effect of the significant refinement and enhanced uniformity of the primary α-Mg and β-$Mg_{17}Al_{12}$ phases achieved by dispersed β-SiC nanoparticles.

The deterioration in the enhancement of ultimate tensile strength and ductility of Mg-12Al-0.2Mn-1.4SiC is probably due to the increase of Si content caused by the reaction of SiC nanoparticles with alloy, resulting in the formation of hard, brittle Mg_2Si intermetallic phases. It was reported that the following reactions (1)-(2) can be observed in the microstructure of metal matrix composite of Mg-Al alloys with SiC particles [18-19].

$$4Al + 3SiC \rightarrow Al_4C_3 + 3Si \quad (1)$$
$$2Mg + Si \rightarrow Mg_2Si \quad (2)$$

It was also found that there is SiO_2 amorphous layer on the surface of some SiC particles [18]. Therefore, other reactions (3)-(4) can occur, supplying more free Si elements to form Mg_2Si phases.

$$2Mg + SiO_2 \rightarrow 2MgO + Si \quad (3)$$
$$Mg + 2Al + 2SiO_2 \rightarrow MgAl_2O_4 + 2Si \quad (4)$$

XRD patterns of pure Mg-12Al-0.2Mn alloy and its nanocomposite with β-SiC nanoparticles are shown in Fig. 7. For the pure alloy, the peaks from Mg and β-$Mg_{17}Al_{12}$ phases are clearly displayed. In the case of SiC nanocomposites, small peaks from Mg_2Si phase can be detected. In addition, the peak intensity of Mg_2Si phase in the nanocomposite with 0.9 wt.% SiC

nanoparticles was obviously weaker than that in the 1.4 wt.% SiC nanocomposite.

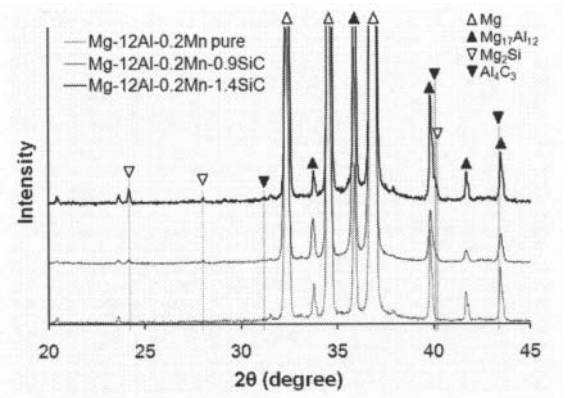

Figure 7. XRD patterns of Mg-12Al-0.2Mn pure alloy and its SiC nanocomposites.

As shown in Fig. 8, SEM photograph of Mg-12Al-0.2Mn-1.4SiC nanocomposite also shows the massive Mg_2Si phase at the grain boundary adjacent to β-$Mg_{17}Al_{12}$ intermetallic phases. It is also observed that SiC nanoparticles are located not only in the massive Mg_2Si but inside some $Mg_{17}Al_{12}$ phases. Furthermore, it is found that some α-Mg phases contain β-SiC nanoparticles.

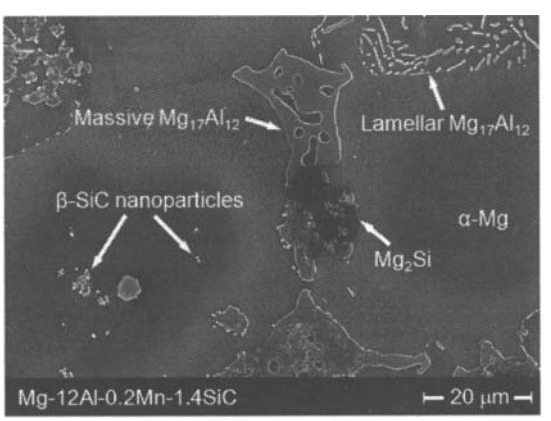

Figure 8. SEM photographs of Mg-12Al-0.2Mn-1.4SiC nanocomposite.

Conclusions

Simultaneous refinement of primary α-Mg and β-$Mg_{17}Al_{12}$ phases is achieved in Mg-12Al-0.2Mn alloy with the addition of β-SiC nanoparticles with a diameter of 50 nm. The primary α-Mg phases are refined from the dendrite to the globular equiaxed grain. The refining effect does not change significantly when β-SiC nanoparticle content is increased from 0.9 to 1.4 wt.%. The average grain size of primary α-Mg in Mg-12Al-0.2Mn-0.9SiC nanocomposite is about two times smaller than that of pure Mg-12Al-0.2Mn alloy. The massive β-$Mg_{17}Al_{12}$ phases are also significantly refined with the addition of β-SiC nanoparticles. The large continuous network phases are modified into discrete thin ones. The mechanical properties of Mg-12Al-0.2Mn alloy are improved with the addition of β-SiC nanoparticles. For Mg-12Al-0.2Mn-0.9SiC nanocomposites, the ultimate tensile strength increased by 14% and the ductility is improved by 71%, while the yield strength is increased by about 8%. The enhancement of yield strength in Mg-12Al-0.2Mn-1.4SiC nanocomposite was limited by the formation of hard brittle Mg_2Si phases by the reaction of nanoparticles with alloy.

Acknowledgments

This work is sponsored by National Institute of Standard and Technology through its Technology Innovation Program. In addition, the authors express their gratitude to US Magnesium LLC. for materials donation.

References

1. A. Rudajevova, M. Stanek, and P. Lukac, "Determination of thermal diffusivity and thermal conductivity of Mg-Al alloys," *Mater. Sic. Eng. A*, 341 (2003), 152-157.
2. M.X. Zhang annd P.M. Kelly, "Crystallography of Mg17Al12 precipitates in AZ91D alloy," *Scr. Mater.*, 48 (2003), 647-652.
3. G. Song, A.L. Bowles, and D.H. St. John, "Corrosion resistance of aged die cast magnesium alloy AZ91D," *Mater. Sci. Eng. A*, 366 (2004) 74-86.
4. A. Pardo, M.C. Merino, A.E. Coy, F. Viejo, R. Arrabal, and S. Feliu Jr., "Influence of microstructure and composition on the corrosion behaviour of Mg/Al alloys in chloride media," *Electrochin., Acta.,* 53 (2008) 7890-7902.
5. K. Kubota, M. Mabuchi, and K. Higashi, "Processing and mechanical properties of fine-grained magnesium alloys," *J.Mater. Sic.*, 34 (1999) 2255-2296.
6. F. Czerwinski, *Magnesium Injection Molding* (New York, NY: Springer, 2007), 19-41.
7. Y.C. Lee, A.K. Dahle, and D.H. St. John, "The role of solute in grain refinement of magnesium," *Metal. Mater. Trans. A*, 31 (2000) 2895-2905.
8. Y. Guangyin, S. Yangshan, and W. Zhen, "Effect of antimony on microstructure and mechanical properties of Mg-9Al based alloy," *J. Nonferrous Metals,* 9 (1999) 779-784.
9. Y. Lu, Q. Wang, X. Zeng, W. Ding, C. Zhai, and Y. Zhu, "Effects of rare earths on the microstructure, properties and fracture behavior of Mg–Al alloys," *Mater. Sci. Eng. A*, 278 (2000) 66-76.
10. S. Zhang, W. Li, K. Yu, and D. Tan, "The grain refinement processes of magnesium alloys," *Foundry*, 7 (2001) 373-375.
11. Z. Trojanova, P. Lukac, H. Ferkel, B.L. Mordike, and W. Riehemann, "Stability of Microstructure in Magnesium Reinforced by Nanoscaled Alumina Particles," *Mater. Sci. Eng. A*, 234–236 (1997) 798–801.
12. J. Lan, Y. Yang, and X. Li, "Microstructure and microhardness of SiC nanoparticles reinforced composite fabricated by ultrasonic method," *Mater. Sci. Eng. A*, 386 (2004) 284-290.
13. G. Cao, J. Kobliska, H. Konishi, and X. Li, "Tensile properties and microstructure of SiC nanoparticle-reinforced Mg-4Zn alloy fabricated by ultrasonic cavitation-based solidification processing," *Metal. Mater. Trans. A*, 39 (2008) 880-886.
14. M. DeCicco, H. Konishi, G. Cao, H. Choi, L. Turng, J. Perepezko, S. Kou, R. Lakes, and X. Li, "Strong, ductile magnesium-zinc nanocomposites," *Metal. Mater. Trans. A*, 40 (2009) 3038-3045.
15. P.S. Robi, B.C. Pai, K.G. Satyanarayana, S.G.K. Pillai, and P.P. Rao, "The Role of surface treatments and magnesium

additions on the dispersoid matrix interface in cast Al-Si-Mg-15 wt-percent SiCp composites," *Mater. Charact.*, 27 (1991) 11-18.
16. D.Y. Ying and D.L. Zhang, "Processing of Cu–Al_2O_3 metal matrix nanocomposite materials by using high energy ball milling," *Mater. Sic. Eng. A.*, 286 (2000) 152-156.
17. G. Gao, H. Choi, H. Konish, S. Kou, R. Lakes, and X. Li, "Mg-6Zn/1.5%SiC nanocomposites fabricated by ultrasonic cavitation-based solidification processing," *J. Mater. Sci.*, 43 (2008) 5521-5526.
18. M.C. Gui, J.M. Han, and P.Y. Li, "Microstructure and mechanical properties of Mg-Al9Zn/SiCp composite produced by vacuum stir casting process," *Mater. Sci. Technol.*, 20 (2004) 765-771.
19. M.A. Easton, A.Schiffl, J. Yao, and H. Kaufmann, "Grain refinement of Mg-Al(-Mn) alloys by SiC additions," *Scripta Mater.*, 55 (2006) 379-382.
20. M.C. Gui, D.B. Wang, J.J. Wu, G.J. Yuan, and C.G. Li, "Microstructure and mechanical properties of cast (Al–Si)/SiC_p composites produced by liquid and semisolid double stirring process," *Mater. Sci. Technol.*, 16 (2000) 556-563.